Structural Studies and Stability of Cluster-like Ru_xSe_y Electrocatalysts

Fabrice Dassenoy and Walter Vogel

Fritz-Haber-Institut der Max-Planck-Gesellschaft, Faradayweg 4-6, 14195 Berlin, Germany

Nicolás Alonso-Vante*

Laboratory of Electrocatalysis, UMR CNRS 6503, Université de Poitiers, 40 Avenue du Recteur Pineau, F-86022 Poitiers Cedex, France

Received: June 18, 2002

Structural studies and stability of cluster-like particles of Ru_x and Ru_xSe_y were performed in situ via X-ray diffraction at wide angles (WAXS). Both materials have a similar particle size (1.4−1.6 nm) in the reduced state. Whereas Ru_x particles are rather sensitive to oxygen from air, the chemical stabilization, against oxidation, of such metallic centers is obtained by the coordination of selenium atoms. The role of selenium atoms is also to stabilize the nanostructural nature (geometric effect) of the compound, as demonstrated by the temperature measurements (up to 300 °C) in the gas phase, and to provide the electronic effect for electrocatalysis.

1. Introduction

Ruthenium is an important catalyst in the chemical industry, having applications in hydrogenolysis,[1] in hydrogenation of benzene,[2] in Fischer−Tropsch synthesis,[3] and as a catalyst for ammonia synthesis.[4] Furthermore, it is one of the most active metals for oxidation reactions.[5,6] It has also been proved that ruthenium-based catalyst cluster materials are effective cathodes for the molecular oxygen reduction in acid medium and have the advantage of being very selective in the presence of methanol.[7−9] In this line of research, a series of chalcogenide compounds (Ru_xX_y, X = S, Se, and Te) have been synthesized and tested for the same electrochemical process.[10] Ru_xSe_y resulted in being the most active one. With EXAFS measurements, it has been determined that the chalcogen, e.g., S, blocks the catalytic centers of ruthenium.[11] The beneficial effect of coordinating selenium atoms to ruthenium has been reported some years ago on molybdenum-containing Ru_xSe_y compounds.[12] Such compound, in thin layer form, exposed to oxygen from air, did not lead to the formation of selenium oxides as revealed by XPS measurements. Attempts to explain the influence of selenium onto the ruthenium cluster structure were reported recently.[13,14]

The aim of the present work is to further investigate the structure of such catalysts (Ru_xSe_y) with special attention to the distribution of the Se atoms in the particles. The gas phase study of Ru_xSe_y particles in the presence of oxygen was also performed and the results compared with those obtained from pure Ru_x particles. The comparison of the evolution of the structural characteristics of the particles during the treatment of oxidation should help to determine the distribution of the Se atoms in the particles.

2. Experimental Section

2.1. Sample Preparation. The Ru_x and Ru_xSe_y particles were elaborated under mild conditions in organic solutions, from transition metal carbonyl complexes, as described, e.g., in refs 8, 12, and 15.

Summarizing, for Ru_x,[8] the chemical precursor ($Ru_3(CO)_{12}$, from Alpha no. 617002) was dissolved in 1,2-dichlorobenzene (Dcb, Merck No. 6.03298.1000) and reaction was performed in nitrogen atmosphere under refluxing conditions for 20 h. To synthesize Ru_xSe_y,[12,15] a similar procedure as to that used for Ru_x with addition of selenium was followed. The selenium was from Alpha no. 36208 (<325 Mesh). The Ru_x and Ru_xSe_y powders were recovered by filtration on a 0.2 μm PTFE filter.

2.2. X-ray Diffraction. *2.2.1. X-ray in Situ Measurements.* The diffraction experiments were performed with a Guinier powder diffractometer (HUBER) set at the 45° transmission position. A Johansson type Ge monochromator produces a focused monochromatic Cu Kα_1 primary beam (λ = 0.15406 nm). Structural changes induced by the gas phase reaction were studied with a specially designed in situ cell attached to the goniometer.[16] The two samples were pressed into pellets 8 mm × 10 mm × 0.1 mm in size and fixed between two 0.1 mm beryllium plates before being inserted in the reaction cell. The sample holder was designed to hold both samples and to switch from one to the other at every counting position of the goniometer. The detection of the structural changes in the particles was performed in the so-called open slit (OS) mode with a time resolution of 5 s. The open receiving slit ($\Delta\theta$ = 2°) was set to the position of a specific diffraction peak to monitor the peak intensity. The variations of the intensity were used to observe some phase changes during the treatment. It also provides evidence for the growth of the particles, because a narrowing of the diffraction line induced an increase of the peak intensity. Angular scans were taken intermediately for a full structure analysis. The X-ray patterns were measured with high resolution in the step-scanning mode with a narrow receiving slit (0.125°). Scans were recorded in the theta range 5°−48°, at room temperature and under vacuum (10^{-3} bar). The Be peaks, due to the plates, were cut from the scan. The background-corrected patterns were subjected to the usual angular correction for absorption, polarization, and geometrical

* To whom correspondence should be addressed. E-mail: Nicolas.alonso.vante@univ-poitiers.fr. Fax: 00 30 549 45-3580.

10.1021/jp021443n CCC: $22.00
Published on Web 11/01/2002

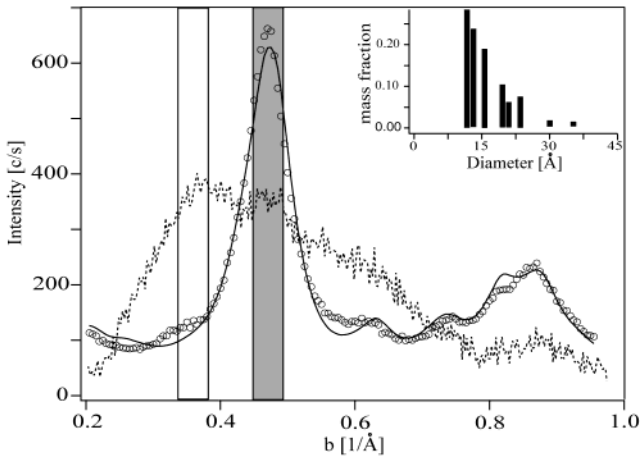

Figure 1. WAXS patterns of Ru_xO_y (Dcb) after 7 months storage in air (dashed line) and of the as synthesized $Ru_xSe_yO_z$ (Dcb) particles (circles line). The solid line is the DFA simulation of the diffraction pattern of $Ru_xSe_yO_z$ (Dcb). The insert to the figure shows the mass fractions of the *hcp* model clusters versus their diameters used for this simulation.

factors, and plotted versus the reciprocal scattering length $b = 2 \sin \theta/\lambda$ (θ, Bragg angle; λ, wavelength). The simulation of the X-ray pattern was performed by the so-called Debye Function Analysis (DFA).

2.2.2. DFA Simulation. This technique constitutes a direct approach to analyze experimental diffraction data from nanoparticles and an opportunity to obtain both the structure and the size distribution of an experimental diffraction profile. This was achieved by comparing linear combinations of Debye functions of a sequence of model particles of different sizes and structures with the experimental function using a nonlinear least-squares parameter fit.[17] This procedure handled the problem of the particle size distribution. Some assumptions about the particles' structure were necessary to perform the simulation. A set of free parameters was used for the number of fractions of the individual clusters. Additional parameters were (i) the exponent of the Debye−Waller factor, (ii) the average spacing within the individual clusters, and (iii) an additive constant correcting for errors in the background subtraction. A complete description of the DFA is found in refs 18 and 19.

3. Results

3.1. Structure of the As-Synthesized Ru_xSe_y and Ru_x Particles. Figure 1 shows the wide-angle X-ray scattering patterns (WAXS) of the as-synthesized Ru_xSe_y particles and of some Ru_x particles (Ru_x-Dcb) after storage for several months in air. The Ru_x particles are not stable under air and fully oxidized when exposed to it for a long period.[8,20] The Ru_{met} peak at $b = 0.48$ Å^{-1} is hardly visible. The diffraction peaks of the Ru_xSe_y particles are well defined. The Debye function analysis (DFA) simulation was applied on this experimental function with a set of Debye functions calculated from *hcp* model clusters with increasing sizes covering the diameter range between approximately 10 and 40 Å. The best DFA fit is superimposed in Figure 1. The very good agreement between the two functions reveals the uniqueness of the structure. It also constitutes a good proof of the metallic character of the particles, because no separate Se-containing phase is observed. The small peak observed at 0.38 Å^{-1} reveals, nevertheless, a weak oxidation of the surface of the particles, which is far from being comparable to that of the pure Ru_x particles. The presence of oxygen was detected some time ago via Rutherford backscattering (RBS).[12] That is why such a transition metal compound was named $Ru_xSe_yO_z$ or when it contained molybdenum $(Ru_{1-x}Mo_x)_ySeO_z$. The size histogram of the $Ru_xSe_yO_z$ particles shown in the insert indicates a relatively broad size distribution and a mean diameter of 15 Å. In addition, an expansion of 0.49% of the mean metal−metal distance in the chalcogenide particles, in comparison with this distance in the Ru bulk material, was observed.

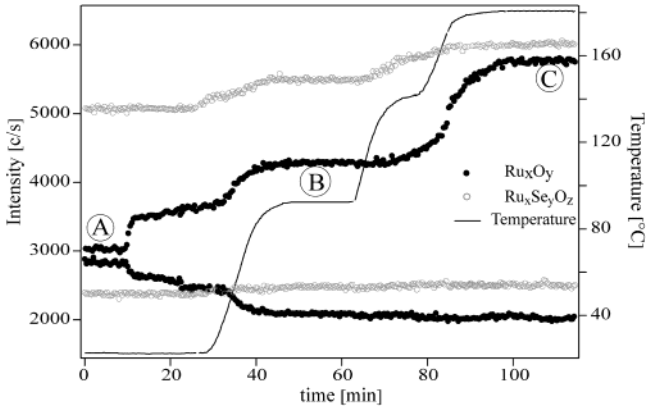

Figure 2. Direct in situ comparison of the gas-phase reduction of Ru_xO_y and $Ru_xSe_yO_z$ particles. The diffracted intensities around the oxide peaks (lower curves) and the main metal peaks (upper curves) are measured versus time and increasing temperature (solid line).

3.2. Reduction of the Ru_xO_y and $Ru_xSe_yO_z$ Particles. The in situ reduction treatment was performed simultaneously on both systems. The in situ X-ray diffraction technique allows the direct comparison of Ru_xO_y and $Ru_xSe_yO_z$ samples at identical reducing conditions. The receiving slit of the diffractometer was set at $\theta = 16°$ ($b = 0.36$ Å^{-1}), the diffraction angle of the ruthenium oxide peak. After a 5 s counting time, for both samples, with sample exchange, the diffraction angle was changed to $\theta = 22°$ ($b = 0.48$ Å^{-1}), the ruthenium metal peak position. These slit positions are indicated in Figure 1 by a white and a grayish bar, respectively. This procedure was repeated while the treatment conditions were changed. The reduction was performed in 1 bar of hydrogen and at temperatures of up to 180 °C.

Figure 2 shows such time-resolved XRD signals (Ru_xO_y, full circles; $Ru_xSe_yO_z$, open circles). It is worth mentioning that the XRD pattern on $Ru_xSe_yO_z$ did not change with time. For an ongoing reduction, the oxide peak (lower intensity lines) decreases, whereas the metal signal (higher intensity lines) increases. This behavior is already observed for the Ru_xO_y sample at room temperature as soon as the hydrogen is introduced into the cell. The process of reduction is however not complete at room temperature. An annealing of the sample at 90 °C leads to a totally reduced material.

Contrary to the pure ruthenium particles, the signal of the $Ru_xSe_yO_z$ particles at $\theta = 16°$ is very diffuse and not intense because of the weak oxidation of the surface. This explains why from room temperature up to 90 °C no evolution of the intensity at $\theta = 16°$ is observed for the chalcogenide sample. The particles are nevertheless reduced. The diffractograms of the reduced Ru_x and Ru_xSe_y particles recorded at point B in Figure 2 are reported in Figures 3b and 4b, respectively. The experimental function of the chalcogenide particles (Figure 4b) does not show traces of oxides. Moreover, the structural characteristics of the particles are still the same as those of the as-synthesized one (Figure 4a). The diffraction pattern of the Ru_x particles (Figure 3b) looks now very similar to that of the

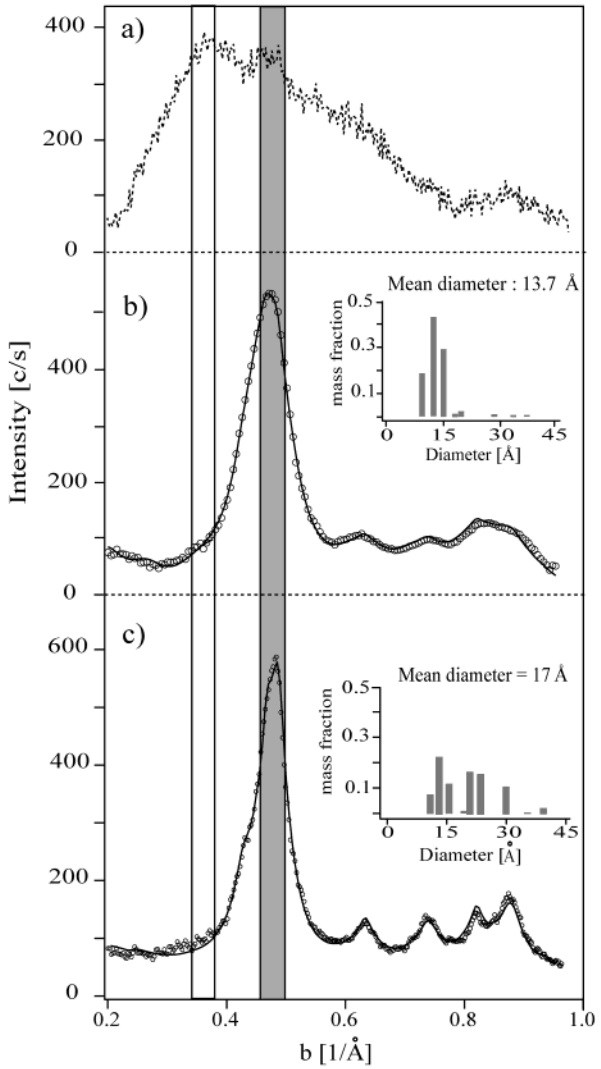

Figure 3. WAXS patterns (dashed and circles lines) of the Ru_xO_y particles at different degrees of reduction in hydrogen. (a) Ru_x after seven months storage in air, (b) reduction under 1 bar of H_2 at 90 °C, (c) reduction under 1 bar of H_2 at 180 °C. The solid lines represent the DFA simulations of the diffraction pattern of the sample. The inserts to the figures show the mass fraction of the *hcp* model clusters Ru_x versus their diameters used for the simulations. The bars indicate the open slit position (see text).

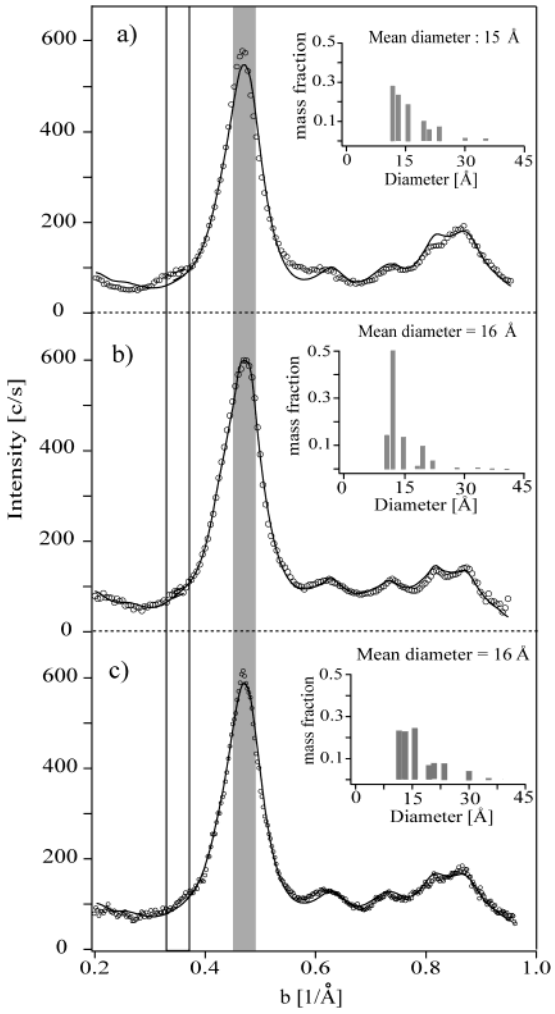

Figure 4. WAXS patterns (circles lines) at different degrees of reduction in hydrogen of the $Ru_xSe_yO_z$ particles. (a) As synthesized particles, (b) reduction under 1 bar of H_2 at 90 °C, (c) reduction under 1 bar at 180 °C. The solid lines represent the DFA simulation of the diffraction pattern of the sample. The inserts show the mass fraction of the *hcp* model clusters Ru_x versus their diameter used for the simulation. The bars indicate the open slit position (see text).

Ru_xSe_y particles recorded at the same step of treatment. The particles are fully reduced. The DFA simulation indicates, however, that the mean diameter of the Ru_x particles is slightly lower than that of the chalcogenide ones (13.7 Å against 16 Å).

A second increase of temperature from 90 to 180 °C produces a further slight increase of the Ru_x particle size, whereas the mean diameter of the chalcogenide particles remains unchanged. The diffractograms of the Ru_x and Ru_xSe_y particles, recorded at the end of the treatment (point C in Figure 2), are reported in Figures 3c and 4c. The size distributions obtained from the DFA simulations are similar for both systems. The mean diameter is still of 16 Å for the Ru_xSe_y particles, whereas it is close to 17 Å for the Ru_x particles. The mean metal−metal distance in the Ru_x particles is the same as in the bulk material, whereas this distance is still expanded by 0.48% in the Ru_xSe_y particles.

So far, this investigation performed on Ru_x and Ru_xSe_y allowed us to clearly identify the structure of the as-synthesized and reduced particles and indicates the stability property of the Ru_xSe_y clusters. Nevertheless, no information concerning the distribution of Se in the clusters had been obtained. To answer this question, the two systems which now present the same structural characteristics (totally reduced, same structure, and same mean diameter) were exposed to an oxidation treatment. As before, the structural evolution of the particles during the treatment was followed by in situ XRD and then compared.

3.3. Oxidation of the Ru_x and Ru_xSe_y Particles. The prereduced particles were exposed to 1 bar of flowing pure oxygen at different temperatures. Figures 5a and 5b show the comparison of the gas-phase oxidation of the Ru_x and Ru_xSe_y particles. The diffracted intensities were measured versus time and temperature (i) at the main metal peak ($\theta = 22°$, gray circles), (ii) around the halo of amorphous surface oxide of RuO_x and $Ru_xSe_yO_z$ ($\theta = 16°$, full circles), and (iii) at the main peak of the rutile phase of RuO_2 ($\theta = 14°$, open circles in Figure 5a). A grayish, a white, and a hashed bar respectively indicate the positions on the diffractograms in Figures 6a and 7a.

3.3.1. Interpretation of the in Situ Oxidation. (a) Pure Ruthenium Particles (Figure 5a). In what concerns the Ru_x particles, under 1 bar of O_2, from ambient temperature up to 160 °C, the intensity of the prominent metal peak decreases as well as the intensities of the oxide peaks which increase

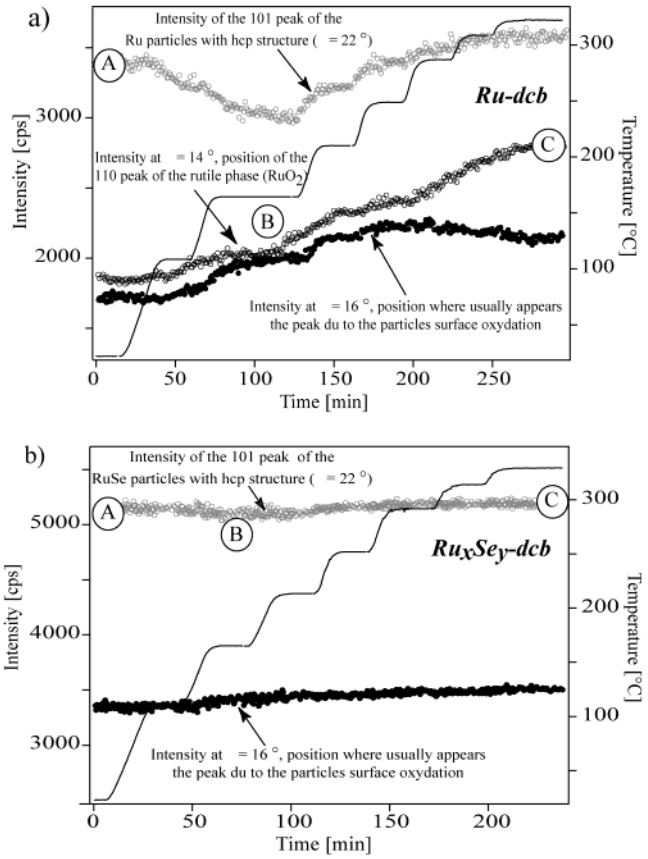

Figure 5. In situ comparison of the gas-phase oxidation of Ru_x (a) and Ru_xSe_y (b). The diffracted intensities of the main metal peak at $\theta = 22°$ (grey circles), around the halo of amorphous surface oxide of RuO_x and $Ru_xSe_yO_z$ (full circles), and of the main peak of the rutile phase of RuO_2 at $\theta = 14°$ (open circles) are measured versus time and increasing temperature (solid line).

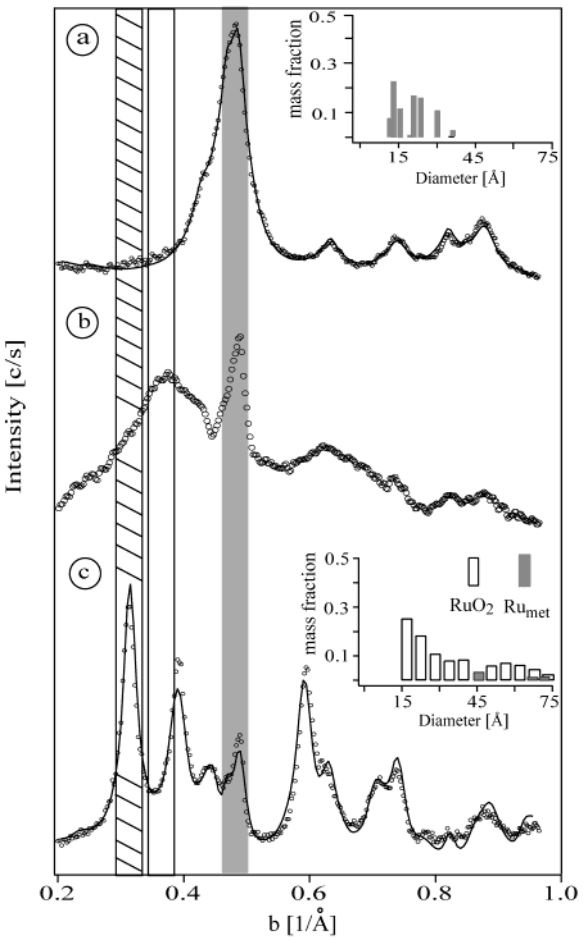

Figure 6. WAXS patterns (open circles) at different degrees of oxidation of the Ru_x particles. (a) Prereduced particles, (b) oxidation under 1 bar of O_2 at 160 °C, (c) oxidation under 1 bar of O_2 at 320 °C. The solid lines represent the DFA simulations of the diffraction pattern of the sample. The inserts show the mass fraction of the *hcp* model clusters Ru_x versus their diameters used for the simulations.

concomitantly. Such evolution indicates the process of oxidation of the particles. The diffractogram recorded at point B and reported in Figure 6b confirms a strong oxidation of the surface of the particles which is characteristic for the presence of a diffuse halo centered around the position $b = 0.36$ Å^{-1}. The main metal peak of the Ru_x particles is still visible. This means that either the particles are oxidized at the surface and preserve a metallic core or that a mixture of small totally oxidized particles and larger metallic particles compose the system. The increase of the intensity at $\theta = 14°$ observed in Figure 5a between 25 and 160 °C is not significant at this step of the treatment. The diffractogram of Figure 6b clearly shows that the measured intensity corresponds, in fact, to that of the shoulder of the oxide surface peak.

Above 160 °C, however, the intensity of the metal peak progressively increases. As mentioned above, this increase is related to a growth of metallic particles because of the thermal effect. At the same time, the intensities of the oxide peaks continue to increase. Above 250 °C, the intensity of the oxide surface peak stabilizes, but the rutile phase peak continues to increase with temperature. Finally, oxidation becomes nearly total and the highly disordered (amorphous-like) preformed RuO_x phase is converted into nanocrystalline RuO_2. This is evidenced by the diffractogram (Figure 6c) recorded at the end of the treatment (at point C in Figure 5a). The DFA simulation (solid line) was performed with RuO_2 Debye functions. It shows that ~95% of the particles are now totally oxidized and that about 5% are the contribution of metallic particles. The size histogram of the particles is inserted in Figure 6c. The mean diameter of the RuO_2 particles is of 32 Å.

(b) Chalcogenide Particles: Ru_xSe_y. Figure 5b shows that, independent of the temperature, the Ru_xSe_y particles behave in a completely different manner: the intensities of the two successive peaks are perfectly stable in an oxygen environment. In fact, the diffractograms recorded at 160 and 325 °C (parts b and c of Figure 7) show identical patterns, similar to those of the as-synthesized particles. A shoulder at $b = 0.36$ Å^{-1}, comparable to that observed on the pattern of the as-synthesized particles, indicate, however, a weak oxidation of the surface of the particles. This shoulder is more pronounced at the end of the treatment, but the oxidation is still restricted to the surface of the particles. The metal−metal distance in the particles is still the same as in the native particles and slightly expanded to 0.5% against pure bulk ruthenium at the end of the treatment.

4. Discussion

4.1. Ru_x versus Ru_xSe_y Clusters. Ru_x clusters synthesized in xylene (Xyl) or in 1,2-dichlorobenzene (Dcb) from the $Ru_3(CO)_{12}$ precursor reacted in a similar way when exposed to oxygen from air. The difference in their reactivity was due to a different degree of disorder Ru_x(Xyl) > Ru_x(Dcb), essentially of the surface atoms, in the nanoscale domain, as discussed by us in a recent publication.[20] Conversely, experimental evidence is given that chalcogenide particles produced from the reaction

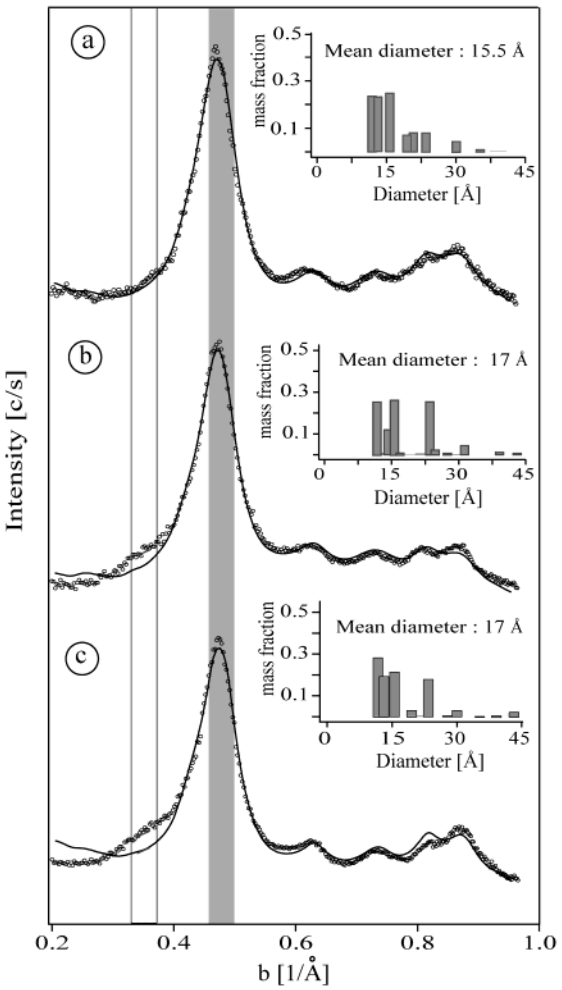

Figure 7. WAXS patterns (open circles) at different degrees of oxidation of the Ru_xSe_y particles. (a) Prereduced particles, (b) oxidation under 1 bar of O_2 at 160 °C, (c) oxidation under 1 bar of O_2 at 320 °C. The solid lines represent the DFA simulations of the diffraction pattern of the sample. The inserts show the mass fraction of the *hcp* model clusters Ru_x versus their diameters used for the simulations.

between $Ru_3(CO)_{12}$ and Se are much more resistant to oxidation than monometallic Ru_x particles with similar size. This phenomenon can be due to the presence of Se atoms coordinated at the surface of the ruthenium atoms, protecting them from oxidation. In fact, the coordination of Se to ruthenium atoms occurs during the first stages of the reaction with $Ru_3(CO)_{12}$, thus, leading to the formation of $Ru_4Se_2(CO)_{11}$.[15,21,22] This molecular cluster is the chemical precursor for Ru_xSe_y. The in situ diffraction patterns (after pyrolysis of $Ru_4Se_2(CO)_{11}$ in gas phase (N_2) at about 210 °C) has recently been studied. After release of the carbonyls, the *hcp*-Ru_xSe_y nanoparticles, similar to those formed in a Dcb solution, cf. Figure 4b, are formed. These results will be submitted in short for publication. In agreement with this observation, no separate Se-containing phase is observed. This is also substantiated by the fact that Ru_x and Se atoms are not miscible in the bulk. A direct proof for this hypothesis using WAXS is, however, not possible because the scattering power of Se ($Z = 34$) is very close to that of Ru ($Z = 44$). Diffraction patterns from a model with a random occupation of the two species are indistinguishable from a surface segregation model of Se. The mean metal−metal distance observed in the pure Ru nanoparticles is the same as in bulk ruthenium. For the Ru_xSe_y particles, an expansion of 0.48% of the average metal−metal distance compared to the Ru_x particles of the same size was calculated. This distance was

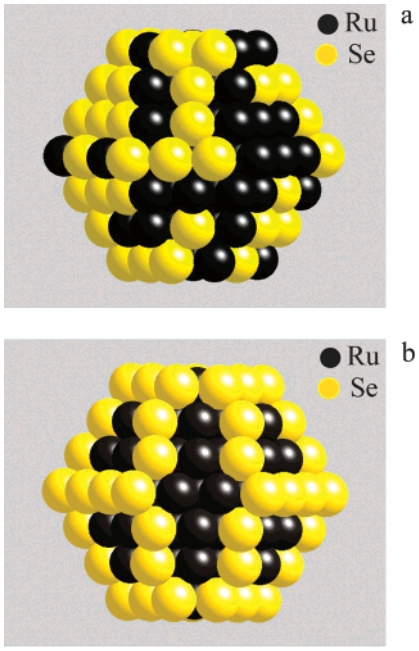

Figure 8. Cluster model structure for $Ru_{99}Se_{54}$ showing the selenium bonding on to the ruthenium clusters: (a) with a statistical distribution; (b) with an ordered positioning.

estimated with an accuracy of ~0.5% by DFA simulations. Within these limits, we could not find evidence for a contraction or expansion of the interatomic distance of the Ru_xSe_y system. We therefore conclude that both the monometallic and chalcogenide particles exhibit an average atomic distance close to that of bulk ruthenium. As revealed by EXAFS analysis,[11,23] the closest metal−metal (Ru−Ru) averaged distance was 2.64 Å and that of the metal chalcogenide (Ru−Se) was 2.43 Å. It is worth noting that the calculated Debye−Waller parameters (degree of disorder)[23] was a factor of 2 higher for the Ru−Se coordination distance than for Ru−Ru. Considering a particle diameter of 17 Å (cf. Figure 4), a pure ruthenium cluster-like model particle could contain 153 atoms (Ru_{153}). This is the third species in a series of *hcp* closed shell clusters with "magic" numbers 13, 57, 153, 323, etc. Therefore, within the *hcp* cluster model (17 Å particle size, 153 atoms), the number of ruthenium atoms available for (electro)catalytic purposes at the surface of such cluster can be $153-57 = 96$. Because $x = 2$ and $y = 1$ in the chalcogenide material, Ru_xSe_y,[15,21] the cluster model could for example contain 99 Ru atoms and 54 Se atoms. According to the present study and the increased disorder of selenium atoms, deduced from EXAFS calculations,[23] these Se atoms are mainly coordinated to surface sites of the ruthenium atoms on the cluster in a statistical way. Figure 8 depicts such an *hcp* cluster model $Ru_{99}Se_{54}$, with (a) all 54 Se atoms replacing surface Ru atoms at random and (b) all 54 Se atoms replacing surface Ru atoms in a regular way, i.e., those that are 5-, 6-, and 7-fold coordinated.

For materials synthesized from the same solvent (either xylene or dichlorobenzene), this result may explain the observed differences in the capacitance values between Ru_x and Ru_xSe_y ($C_{Ru_x} \sim 2C_{Ru_xSe_y}$).[21] In fact, assuming a similar particle size, the 96 surface atoms of Ru_x are about 2.3 times that of Ru_xSe_y, and therefore, the interfacial process, in both catalysts, is governed by the ruthenium surface atoms.

4.2. On the Origin of Ru_xSe_y Clusters Stability. Besides the very good resistance against oxidation of the chalcogenide particles, pointed out in an earlier work,[12] this study puts in evidence the remarkable thermal stability of these particles. Even

under reducing conditions (under hydrogen) and temperatures of up to 180 °C, the particles remain stable and do not significantly grow (cf. Figures 3 and 4). Under oxidation conditions (pure oxygen), there is no evidence of particle size increase (at least up to 160 °C, cf. Figure 7c). However, as discussed above, some catalytic centers must be available in the chalcogenide system. Furthermore, the interaction of oxygen with ruthenium leads to the formation of an oxide-like species (Ru_xO_y; Figure 7). Although the conditions here are far from being compared to an electrochemical system, we believe that this effect is essentially of the same nature to that of coordinated oxygen from water or from dissolved oxygen in the electrolyte.[23] In comparison to Ru_x, which readily transforms to amorphous-like Ru_xO_y (Figure 6b), and to a bulk oxide RuO_2 with rutile structure above $T \approx 250$ °C (Figure 6c) and in which there is growth of particles, the question is raised: Where does this remarkable stability of Ru_xSe_y come from? Why does oxygen preferentially coordinate to ruthenium despite the prominent presence of selenium atoms on the surface? Testing the hypothesis of nonreactivity of selenium with oxygen, the Debye function of a long chain of selenium oxide (SeO_2) able to cover the surface of the chalcogenide particles was simulated. The obtained pattern could not account for the shoulder observed at 0.36 $Å^{-1}$ on the experimental function. This confirms the coexistence of Se and Ru atoms on the surface of the particles and that an amorphous-like ruthenium oxide is formed. Our present results do not support the conclusions reported elsewhere[14] that an amorphous layer of Ru-carbido complexes with CO ligands around the Ru core of the particle forms the active part of the catalyst and that Se acts as a bridge between the core and the catalytic active center. However, in the frame of our experimental evidence, selenium already coordinated to ruthenium in the molecular cluster must change profoundly the electronic nature of the cluster. Besides CO ligand interaction, favorable states are formed between Se 4p and Ru 4d orbitals in the molecular cluster: $Ru_4Se_2(CO)_{11}$. These states are apparently kept when CO ligands released the cluster (via pyrolysis). However, to what extent is the density of state of the ruthenium catalytic center modified? This question cannot be answered up to now; however, it is under investigation.

5. Conclusion

This work shows that the nanostructured chalcogenide compound, Ru_xSe_y, has a remarkable stability against oxidation by virtue of coordinated selenium atoms onto the catalytic center. The coverage of the Ru-cluster surface by selenium atoms (i.e., coexistence with Ru) allows enough free active sites for an efficient electrocatalysis or coordination with oxygen/water.

Acknowledgment. The authors thank the assistance of A.-C. Boucher and T. Lana (University of Poitiers) for the preparation of the samples. One of us (N.A.V.) expresses his thanks to the Alexander von Humboldt Stiftung and the Max Planck Society for funding his stay at the Fritz-Haber-Institut.

References and Notes

(1) (a) Bond, G. C.; Rajaram, R. R.; Yahya, R. *J. Mol. Catal*. **1991**, *69*, 359. (b) Bond, G. C.; Coq, B.; Dutartre, R.; Garcia Ruiz, J.; Hooper, A. D.; Proietti, M. G.; Sanchez Sierra, M. C.; Slaa, J. C. *J. Catal*. **1996**, *161*, 480.

(2) Milone, C.; Neri, G.; Donato, A.; Musolini, M.; Mercandante, L. *J. Catal*. **1996**, *159*, 253.

(3) McQuire, M. W.; Rochester, C. H. *J. Catal*. **1995**, *157*, 396.

(4) Wellenbuscher, J.; Mulher, M.; Mahdi, W.; Sauerlandt, U.; Schutze, J.; Ertl, G.; Schlögl, R. *Catal. Lett*. **1994**, *25*, 61.

(5) Gallezot, P.; Chaumet, S.; Perrard, A.; Isnard, P. *J. Catal*. **1997**, *168*, 104.

(6) (a) Fan, C. Y.; Wang, J.; Jacobi, K.; Ertl, G. *J. Chem. Phys*. **2001**, *114*, 10058. (b) Over, H.; Kim, Y. D.; Seitsonen, A. P.; Wendt, S.; Lundgren, E.; Schmid, M.; Varga, P.; Morgante, A.; Ertl, G. *Science*, **2000**, *287*, 1474.

(7) Alonso-Vante, N. In *Proceedings of the First International Symposium on New Materials for Fuel Cell Systems*; Savadogo, O., Roberge, P. R., Veziroglu, T. N., Eds.; Montréal, Canada, July 9−13, 1995; p 658.

(8) Le Rhun, V.; Garnier, E.; Pronier, S.; Alonso-Vante, N. *Electrochem. Commun*. **2000**, *2*, 475.

(9) Schmidt, T. J.; Paulus, U. A.; Gasteigert, H. A.; Alonso-Vante, N.; Behm, R. J. *J. Electrochem. Soc*. **2000**, *147*, 2620.

(10) Alonso-Vante, N.; Malakhov, I. V.; Nikitenko, S. G.; Savinova, E. R.; Kochubey, D. I. *Electrochim. Acta* **2002**, *47*, 3807.

(11) Malakhov, I. V.; Nikitenko, S. G.; Savinova, E. R.; Kochubey, D. I.; Alonso-Vante, N. *J. Phys. Chem. B* **2002**, *106*, 1670.

(12) Solorza-Feria, O.; Ellmer, K.; Giersig, M.; Alonso-Vante, N. *Electrochim. Acta* **1994**, *39*, 1647.

(13) Bron, M.; Bogdanoff, P.; Fiechter, S.; Dorbandt, I.; Hilgendorff, M.; Schulenburg, H.; Tributsch, H. *J. Electroanal. Chem*. **2001**, *500*, 510.

(14) Tributsch, H.; Bron, M.; Hilgendorff, M.; Schulenburg, H.; Dorbandt, I.; Eyert, V.; Bogdanoff, P.; Fiechter, S. *J. Appl. Electrochem*. **2001**, *31*, 739.

(15) Le Rhun, V.; Alonso-Vante, N. *J. New Mater. Electrochem. Syst.* **2000**, *3*, 331.

(16) Gnutzmann, V.; Vogel, W. *Z. Phys. D; At. Mol. Clusters*, **1989**, *12*, 597.

(17) Marquart, D. M. *J. Soc. Indian Appl. Math*. **1963**, *11*, 431.

(18) Gnutzmann, V.; Vogel, W. *J. Phys. Chem*. **1990**, *94*, 4991.

(19) Vogel, W. *Cryst. Res. Technol*. **1998**, *33*, 1141.

(20) Vogel, W.; Le Rhun, V.; Garnier, E.; Alonso-Vante, N. *J. Phys. Chem. B* **2001**, *105*, 5238.

(21) Le Rhun, V. Ph.D. Thesis, University of Poitiers, Poitiers, France, 2001.

(22) Alonso-Vante, N. "Novel nanostructured material based on transition metal compounds for electrocatalysis" In *Catalysis and Electrocatalysis at Nanoparticle Surfaces*; Wieckowski, W., Vayenas, C., Savinova, E., Eds.; Marcel & Dekker: New York, in press.

(23) Alonso-Vante, N.; Borthen, P.; Fieber-Erdmann, M.; Strehblow, H.-H.; Holub-Krappe, E. *Electrochim. Acta*, **2000**, *45*, 4227.